OBSERVING THE DYNAMICS OF WILDLAND GRASS FIRES

FireFlux—A Field Validation Experiment

BY CRAIG B. CLEMENTS, SHIYUAN ZHONG, SCOTT GOODRICK, JU LI, BRIAN E. POTTER, XINDI BIAN, WARREN E. HEILMAN, JOSEPH J. CHARNEY, RYAN PERNA, MEONGDO JANG, DAEGYUN LEE, MONICA PATEL, SUSAN STREET, AND GLENN AUMANN

The first comprehensive set of in situ measurements of turbulence and dynamics in an experimental wildland grass fire should help improve fire models.

Fire spreading across a prairie during an experimental burn. See Fig. 5 for more details.

Grass fires, although not as intense as forest fires, present a major threat to life and property during periods of drought in the Great Plains of the United States. Recently, major wildland grass fires in Texas burned nearly 1.6 million acres and destroyed over 730 homes and 1320 other buildings. The fires resulted in the death of 19 people, an estimated loss of 10,000 head of livestock, and more than $628 million in damage, making the 2005/06 fire season the worst on record for the state of Texas (Weaver 2006).

Research scientists and engineers have developed various models such as BehavePlus (Andrews et al. 2005), FARSITE (Finney 1998), and Prometheus (Tymstra et al. 2007) to describe fire behavior as an aid to fire management. Most of these models emphasize fuels and basic weather conditions reflected by ▶

surface temperature, humidity, and wind. No operational fire behavior model includes any consideration of the potential role of convective dynamics in fire behavior. A major difficulty in developing realistic fire spread models is the lack of observational data in the immediate environment of wildland fires that can be used for validating these models. This is no great surprise, because making meteorological observations within wildland fires is complicated at best. The possibility of damaging expensive instrumentation is high and the dangers to personnel are too great. Prescribed burns, though, are typically less intense than wildland fires and offer relatively controlled situations in which to conduct measurements. Still, the risk of causing damage to equipment can be high. Very few studies have been able to describe the atmospheric conditions within and during a wildland fire, and even during prescribed burns measurements are very limited (Clements et al. 2006).

Meteorologists and others who study forest and range fires recognize that the existing fire behavior models have limitations that stem from the technology and state of the science when these models were first developed, 20–30 years ago. There is an effort at present to lay the groundwork for a next-generation fire behavior model based more on physics and less on engineering-style parameterized descriptions of the fire environment. The vision for this system includes complex computer models that will capture the effects of atmospheric turbulence, stability, and convective dynamics. Accurate portrayal of these factors requires knowing what happens in nature before it can be included in a computer model, and it is for these reasons that the potential return on any experiments that can quantify them is significant. Better fire behavior models potentially save lives and allow managers to make more informed, scientifically sound decisions.

The International Crown Fire Modeling Experiment (ICFME; Alexander 1998) collected a wide variety data from a number of high-intensity experimental crown fires. Atmospheric measurements included routine weather observations adjacent to the experimental plots along with in situ wind, temperature, and radiation measurements, as well as aerial/surface infrared imagery. This study did not capture high-frequency in situ measurements of flow, temperature, and moisture suitable for examining the turbulent fluxes associated with the burn. However, using high-resolution infrared camera data, Clark et al. (1999) were able to calculate small-scale velocities and heat fluxes from the infrared imagery. This study was most likely the first to investigate the atmospheric dynamics within a fire, and especially that of a crown fire.

Banta et al. (1992) observed the kinematic structure of two forest fire plumes using a Doppler radar for the first and a Doppler lidar for the second. The lidar showed flow convergence and anticyclonic rotation of the near-vertical convection column. They estimated the maximum vertical velocity to be approximately 15 m s^{-1}. Their measurements showed the utility of active remote-sensing platforms for the measurement of fire plumes.

A number of other more recent studies were conducted to better understand wildland fire dynamics such as the Wildfire Experiment (WiFE; Radke et al. 2000), and the FROSTFIRE experiment (Wilmore et al. 1998; Coen et al. 2004), which was conducted to investigate long-term climate effects due to fire. While these experiments used state-of-the-art digital IR cameras, they lacked in situ meteorological measurements. However, Clark et al. (1999) and Coen et al. (2004) did produce detailed analyses regarding heat fluxes and vertical velocities associated with crown fires. The estimated vertical velocities were on the order of 20–30 m s^{-1} and sensible heat fluxes on the order of 11–17 MW m^{-2}. Both of these quantities were derived from IR imagery.

While the FROSTFIRE, WiFe, and ICFME experiments represent some of the more recent and comprehensive studies to date, their ability to characterize fire–atmosphere interactions is limited in some

AFFILIATIONS: Clements, Perna, Jang, Lee, Patel, and Street—Institute for Multidimensional Air Quality Studies and Department of Geosciences, University of Houston, Houston, Texas; Zhong—Department of Geography, Michigan State University, East Lansing, Michigan; Goodrick—Southern Research Station, USDA Forest Service, Athens, Georgia; Li—Institute for Multidimensional Air Quality Studies and Department of Geosciences, University of Houston, Houston, Texas, and Institute for Urban Meteorology, Beijing, China; Potter—Pacific Northwest Research Station, USDA Forest Service, Seattle, Washington; Bian, Heilman, and Charney—Northern Research Station, USDA Forest Service, East Lansing, Michigan; Aumann—Houston Coastal Center, University of Houston, Houston Texas
CORRESPONDING AUTHOR: Dr. Craig B. Clements, Department of Meteorology, San José State University, One Washington Sq., San José, CA 95192-0104
E-mail: clements@met.sjsu.edu

The abstract for this article can be found in this issue, following the table of contents.
DOI:10.1175/BAMS-88-9-1369

In final form 8 March 2007

aspects. First, these studies had limited measurement platforms near or in the experimental fires, and for the instrumentation that was present the sampling frequencies were inadequate for capturing detailed turbulent structures. Second, these studies were conducted in complex combinations of topography and fuels such that the fires were only one of many factors contributing to the turbulence. The simplicity of grass fires in flat terrain provides a better environment for isolating fire–atmosphere interactions. Previous studies conducted in simple grassland plots have focused on fire growth and spread rather than the atmospheric dynamics associated with the fire (Cheney et al. 1993; Cheney and Gould 1995).

Numerical models of coupled fire–atmosphere processes have emerged as viable research tools over the past decade, and grass fires have proven to be a popular choice for initial model testing (Clark et al. 2004; Linn and Cunningham 2005; Sun et al. 2006). While these numerical models make it possible to study the complex interaction between the fire and the ambient atmosphere, the accuracy of these models has not been adequately documented largely because of the lack of appropriate observational datasets, which puts significant limitations on their usage and further improvement. Data on fire perimeter evolution, such as those provided by Cheney et al. (1993) and Cheney and Gould (1995), are largely inadequate for validating these models. Because wildland fire involves processes ranging in scale from submillimeter for combustion to over a kilometer for the convective plume, it is not currently possible to discretely model all relevant scales, forcing many of the processes to be represented as subgrid parameterizations (Sun et al. 2006). The balance between convective and radiative heat transfer that governs the evolution of the fire is largely controlled by these parameterizations. Measurements of atmospheric turbulent fluxes would provide data essential to the development of these parameterizations and supply a better means of validating these models than a simple description of the evolution of the fire perimeter.

In February 2005, a pilot study was conducted to measure fluxes of water vapor, heat, and carbon dioxide associated with a prescribed grass fire (Clements et al. 2006). The study documented these fluxes quantitatively using a 43-m instrumented flux tower within the burn perimeter and a tethered balloon sounding system immediately downwind of the fire. The measurements revealed significant temperature increases (perturbations up to 20°C), heat fluxes (greater than 1000 W m^{-2}), and CO_2 (larger than 2000 ppmv) within the smoke plumes as well as intensification of turbulent mixing. Furthermore, the observations revealed an increase in water vapor mixing ratio of more than 2 g kg^{-1} or nearly 30% over the ambient air. These observations provided direct evidence that natural fuel load grass fire plumes may modify the dynamic environment of the lower atmosphere through not only heat release and intense mixing, but also by a large addition of water vapor.

While this pilot study appears to be one of the first studies to measure in situ turbulence and moisture enhancement within a grass fire, the overall instrumentation and experimental design were not as complete as needed to fully document the nature of the mean and turbulent flows, the plume dynamics, and the fire–atmosphere interactions. Therefore, a more intensive study, called FireFlux, was conducted to collect a more comprehensive set of data for model validation.

SITE, EXPERIMENTAL DESIGN, AND INSTRUMENTATION.

Site description. The experimental burn took place on 23 February 2006 at the Houston Coastal Center (HCC) located in central Galveston County near La Marque, Texas, approximately 45 km southeast of the Houston metropolitan area and 22 km from the western shores of Galveston Bay. HCC has a number of small- to medium-sized prairies that are categorized as Texas Gulf Coast tall-grass prairies consisting of a mixture of native grasses, including big bluestem (*Andropogon gerardi*), little bluestem (*Schizachyrium scoparium*), and long spike tridens (*Tridens strictus*). The experimental prairie (Fig. 1) is 155 acres (0.63 km^2) in size and consists of 90% native species. Typically, the prairie is managed by mowing every year in the fall and prescribed burning every 2–5 years. The prairie was burned the previous year for the pilot study.

Burn plan. The experiment was designed to document the flow and turbulence characteristics of both the fire–atmosphere interface and the plume both within the fire perimeter and downwind of the burn area. The primary goal of the burn was to achieve conditions that mimic that of a wildfire—dry fuel conditions with the fire spread being driven in the direction of the wind. The primary concern in burning this unit is the requirement set forth by the local fire department for burning only on days with northerly flow, to limit smoke impacts on a shopping center located to the north of the HCC.

In preparation for the prescribed burn, HCC mowed the experimental prairie extensively to create

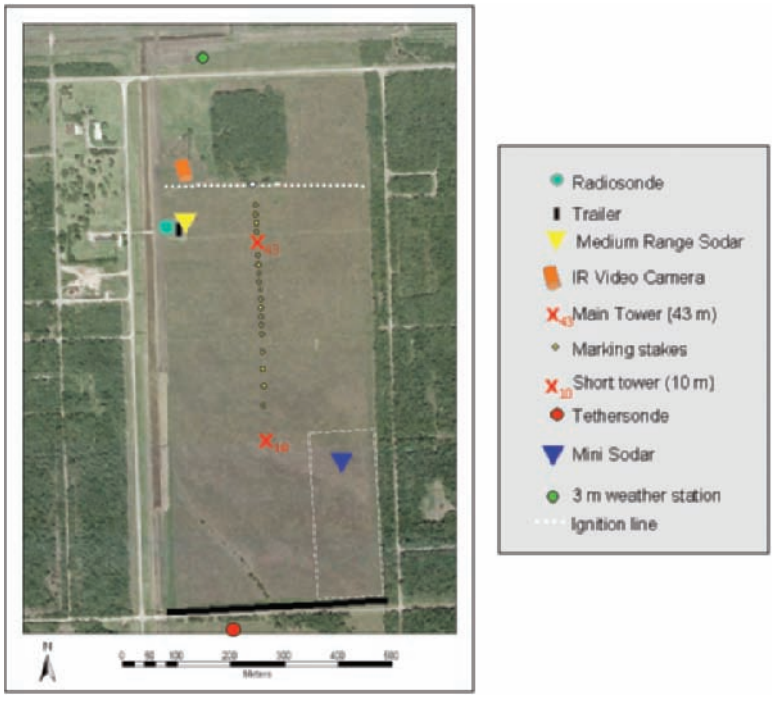

Fig. 1. Map of HCC experimental prairie and layout of instrumentation. White dot in middle of ignition line represents starting point calculated by GPS, black line at southern edge indicates back burn area, and white dashed box indicates area of cut grass.

safety corridors all around the prairie. Initial plans were to simply ignite the field from the upwind edge (i.e., a headfire) and allow it to move past the instrumentation in order to closely simulate a natural grass fire. Because the hope was to burn with moderate winds, the original burn plan did not include any effort to light the downwind edge on fire (i.e., a back burn), which would widen the safety zone on the downwind side of the fire before the subsequent head fire reached that side. However, on the day of the burn, projected fire intensities were at the upper limit of what was deemed acceptable and mandated some black lining along the southern edge of the prairie and around the sodars for increased safety of personnel and equipment. There was no black lining around the towers.

Instrumentation and measurements. The meteorological instrumentation deployed during the experiment included the following:

- tower-based high-frequency turbulence measurements at two locations within the burn perimeter to capture and characterize the turbulent nature of the atmosphere;
- two sodars located on the east and west sides of the burn unit to capture the vertical wind structure;
- a tethered balloon system immediately downwind of the burn unit to describe vertical structure of temperature, humidity, and wind in the fire plume;
- a weather station located approximately 100 m from the northern edge of the prairie to capture undisturbed ambient conditions immediately upwind of the burn unit.

Towers. Two instrumented towers were used for the experiment. The main tower is a 43-m guyed tower located within the prairie approximately 100 m from its northern edge, while the secondary tower located 300 m south of the primary tower was a 10-m portable tower (Fig. 1). Instrumentation for both towers is presented in Table 1. To reduce the risk of instrument damage, the grass around each tower was mowed prior to the burn out to a distance of approximately 5 m from the base and fireproof insulation (Cotronics, Inc.) was wrapped around the base of the towers up to 2.5 m (Fig. 2a). Data were collected using Campbell Scientific, Inc. CR5000 dataloggers and transferred in near–real time to a computer located inside the data acquisition trailer over Ethernet via buried fiber optic cable (43-m tower) and RF modems. High-frequency data from the 10-m tower were stored on a memory card in the datalogger.

Sonic anemometers fail in high-temperature environments. Even so, sonic anemometers are the most economical and suitable in situ platform to measure fluid phenomena that occur on time scales of seconds and minutes, such as wildland and range fires. While micrometeorological flux towers are typically used to study turbulent fluxes of heat, momentum, and water vapor over seasonal and annual temporal scales, the same instrumentation can be used to study the dynamic structure of a grass fire as it spreads through a native fuel bed. In the case of this experiment, heat and temperature extremes associated with the fire caused some instrument failure and minor damage (i.e., broken thermocouples, cabling, etc.). However, these standard instruments performed better than expected and allowed for the first time the collection of valuable observations of the dynamic nature of

Table 1. Tower instrumentation deployed during FireFlux experiment.

Platform	Type	Variables	Measurement height (m AGL)	Sampling frequency
Main tower (43 m)	3D sonic anemometers (R.M. Young 81000)	u, v, w, t_s^a	2.1, 10, 28.5, and 43	20 Hz
	LI-COR 7500 open-path gas analyzers	CO_2 and H_2O	10 and 28.5	20 Hz
	Type T thermocouples (Omega, Inc., 5SC-TT-40)	Temperature	Total of 15 mounted between 0.1 and 43 m	1 Hz
	Type-K fine-wire thermocouple (Omega, Inc., CHAL-0005)	Temperature	2.1 m on sonic anemometer	20 Hz
	Kipp & Zonen CNR1 four-component net radiometer	Net radiation	6.9	1 Hz
	Heat flux plates (REBS, HFT-3)	Soil heat flux	−0.04	1 Hz
	Soil temperature thermocouple probe (CSI TCAV),	Temperature	−0.04	1 Hz
	Soil water content probe (CSI CS-616)	Moisture content	−0.04	1 Hz
	Ceramic type-K thermocouples (Omega, Inc., XC-24-K-12)	Fuel temperature	2.1, 1.73, 1.47, 0.6, 0.13	1 Hz
	R.M. Young 5103 anemometers	Mean wind speed and direction	2, 10, 20, 43	1 Hz
	CSI CS-500 temperature/RH probes	Mean temperature and RH	2, 10, 20, 43	1 Hz
Short tower (10 m)	3D sonic anemometers (R.M. Young 81000)	u, v, w, t_s	2.3, 10	20 Hz
	CSI KH20 hygrometer	Water vapor	2.3	20 Hz
	Vaisala, Inc., HMP45C probe	Mean temperature and RH	2	1 Hz
	Heat flux plates (REBS, HFT-3)	Soil heat flux	−0.04	1 Hz
	Soil temperature thermocouple probe (CSI TCAV),	Temperature	−0.04	1 Hz
	Soil water content Probe (CSI CS-616)	Moisture content	−0.04	1 Hz
	Ceramic type-K thermocouples (Omega, Inc., XC-24-K-12)	Fuel temperature	0.47, 0.89, and 1.4	1 Hz
	Type-T thermocouples Omega, Inc. (5SC-TT-40)	Temperature	2, 5, 10	1 Hz
	Type-K fine-wire thermocouple (Omega, Inc., CHAL-0005)	Temperature	2.3 m on sonic anemometer	20 Hz

t_s^a = sonic temperature
CSI = Campbell Scientific, Inc.

the fire–atmosphere interface before, during, and after the passage of the fire front.

Postprocessing of the sonic anemometer data proved to be a challenge because despiking routines would eliminate most of the observed sharp increases in the wind and temperature fields associated with the fire front passage. Instead, data were bounded by maximum and minimum values that were associated with invalid data. These data were determined by visual inspection of actual instrument output voltages. Eliminated points in the time series were then used to flag data points in other fields. For example, if the recorded voltages were at the maximum of the instrument output, then each variable at that time was flagged and set to "invalid". After the data were bounded, tilt corrections were applied by use of the planar-fit method (Wilczak et al. 2001). Moisture influences on the sonic temperature were corrected following Schotanus et al. (1983).

Sodar systems. Two Doppler sodars were operated for the experiment. A medium-range sodar (Scintec, Inc.,

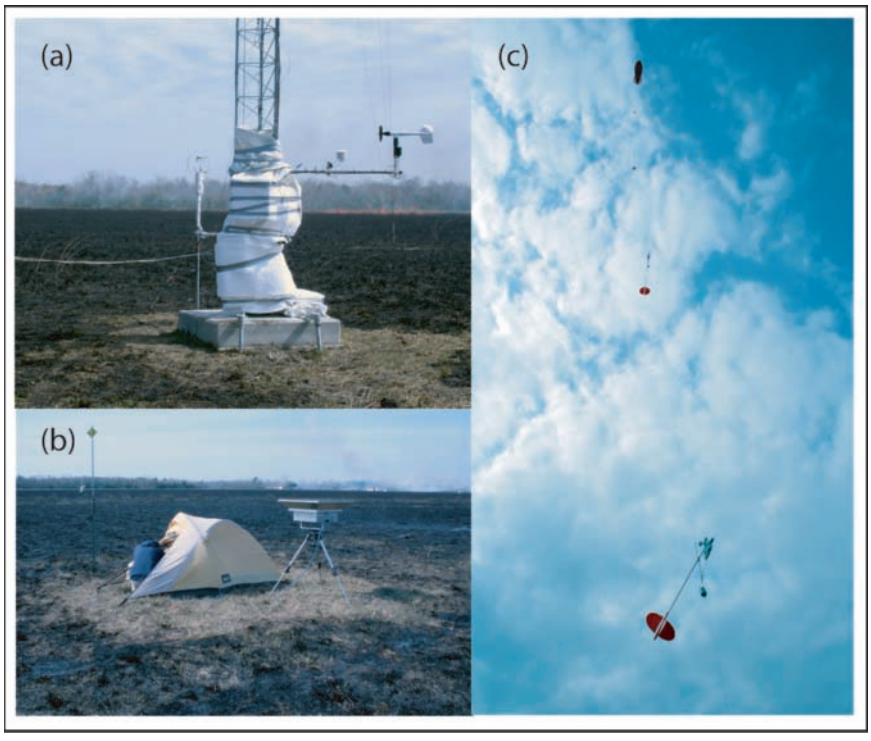

Fig. 2. Photographs of main tower base (a) after burn showing protection around sonic anemometer and tower, (b) mini sodar (Remtech, Inc., PAO) after burn, and (c) tethersonde system deployed in tower mode with five sondes.

MFAS-64) is operated continuously on site next to the prairie, consistently providing wind profiles at 10-m vertical intervals from the first gate (set at 30 m AGL) up to 600 m AGL. The minimum averaging period for this sodar was 10 min. The second sodar deployed for the experiment was a mini sodar (Remtech, Inc., PAO; Fig. 2b) and was operated on the day of the burn starting at 0600 Central Standard Time (CST). This sodar was positioned approximately 150 m east of the south tower in the cut area.

Soundings and tethersonde system. An RS-92 GPS radiosonde was launched on site at 0655 CST on the morning of the burn to document the background atmospheric conditions for the burn. The tethersonde system (Vaisala, Inc.) was used in the tower mode (Fig. 2c) with five sensors located at fixed heights of 3, 10, 50, 80, and 130 m AGL, respectively. The sensors can measure winds, temperature, and humidity at 1-Hz sampling rate, but with five sensors this sampling rate was reduced due to the time required to sequence through each sensor.

Weather station. Background meteorological measurements were made using a basic weather station located upwind and outside of the burn perimeter (Fig. 1). This site consisted of a 3-m tripod that included a Vaisala, Inc., HMP45C probe to measure temperature and relative humidity and R.M. Young 3001 cup and vane sensors to measure wind speed and direction. Data were sampled at 1 Hz and stored as 1-min averages to a CR-23X datalogger.

In addition to these meteorological instruments, a digital infrared video camera, digital SLR camera, and multiple digital video cameras were used to document fire behavior and fire spread rate. Orange markers were placed in the fuel at 10-m intervals from 50 m north to 300 m south of the main tower to aid in spread rate determination.

PRELIMINARY RESULTS. *Fuel conditions and fire behavior.* On the day before the burn, total fuel loading (mass of fuel per unit area) was estimated through destructive sampling of ten 0.38 m × 0.38 m plots. Locations of the 10 samples were determined via a random walk process. The mass of the 10 samples is given in Table 2. Based on these samples, the fuel loading for the burn unit is estimated to be 1.08 kg m^{-2} (or 4.8 tons $acre^{-1}$), which is more than 50% higher than the 3.0 tons $acre^{-1}$ of the standard tall-grass fuel model (fuel model 3 in Anderson 1982).

Table 2. Mass of fuel samples

Sample	Mass (kg)
1	0.171
2	0.137
3	0.149
4	0.130
5	0.239
6	0.137
7	0.224
8	0.127
9	0.193
10	0.066
Mean	**0.157**

Fuel moisture content (the ratio of the difference between the wet and oven-dried weights to the oven-dried weight) was measured for three of the above samples plus a fourth

sample collected the morning of the burn (Table 3). Note that these samples were not exclusively dead vegetation as all fuels (live + dead) within the sample plot were collected. Live fuel was estimated to constitute between 3% and 5% of the total fuel load. Since live fuel moisture values are typically much higher than dead values, a small percentage of live fuel can dominate the measurement. Assuming 4% of the fuel collected was live with a moisture content of 200%, the dead fuel moisture content can be estimated to be between 11% and 19%. Using temperature and humidity observations (14.5°C and 80%) from the morning of the burn (0900 CST) and the fine fuel moisture tables of the fire behavior appendix of the National Wildfire Coordinating Group Fire line Handbook, the dead fuel moisture content is estimated to be 13% at the time of sampling, which is in good agreement with the measured data when the live fuel component is considered. Continued drying of the fine dead fuels as estimated from the tables indicates that dead fuel moisture levels were approximately 9% at the time of the burn (temperature of 17.7°C and relative humidity of 63%).

Fire behavior (rate of spread, flame length, and heat release per unit area) was estimated using the BehavePlus application (Andrews et al. 2005) and observed weather conditions at the time of the burn. Using the average wind speed measured at 2 m (3 m s^{-1}), the predicted rate of spread for the fire is 0.68 m s^{-1} with a flame length of 5.1 m and an estimated heat released in the flaming area of 11.4 kJ m^{-2}. With this rate of spread, the estimated time to burn the study area is approximately 18 minutes, with the fire reaching the main tower in approximately 3.3 minutes.

Using an abandoned tower near the northwest corner of the burn unit, images from a digital infrared video camera located approximately 10 m AGL were used to document the early stages of the fire development just after ignition (Fig. 3). Figure 4a shows the development of the fire one minute after ignition began. Images in Figs. 4b,c,d occur at 10-s intervals thereafter. Maximum temperatures recorded during this 40-s period ranged from 752°C in Fig. 4a to 834°C in Fig. 4d. Peak fire temperatures showed similar variability as the fire approached the main tower approximately 3 minutes after ignition, ranging from 767° to 835°C, with an average of 809°C.

Table 3. Fuel moisture subsamples.

Sample	Wet mass (kg)	Dry mass (kg)	Fuel moisture (%)
3	0.149	0.118	26.3
6	0.137	0.111	23.4
9	0.193	0.158	22.2
Day of burn	**0.154**	**0.130**	**18.5**

The evolution of fire behavior and fire line propagation was documented with time lapse photography using a tripod-mounted digital SLR camera (Canon Rebel XT). The camera was focused on the main tower, including the markers north and south. Figure 5 shows a photo time series of the head fire as it approached and passed the main tower. The time listed in each panel in Fig. 5 corresponds to the datalogger time on the tower. In the first panel (1246:02 CST), the head fire is approximately 45 m from the tower and there is significant smoke and soot in the plume, which is tilted in the downwind direction. At this time, most of the plume impinges on the upper levels of the tower. This can be compared with thermocouple measurements shown in Fig. 6. In Fig. 6a, the temperature increase of the upper plume is not as strong as observed at the lower levels due to the entrainment of environmental air

Fig. 3. Photograph of westward ignition (1243:30 CST). The 43-m main tower is shown in the background. Photo by Glenn Aumann.

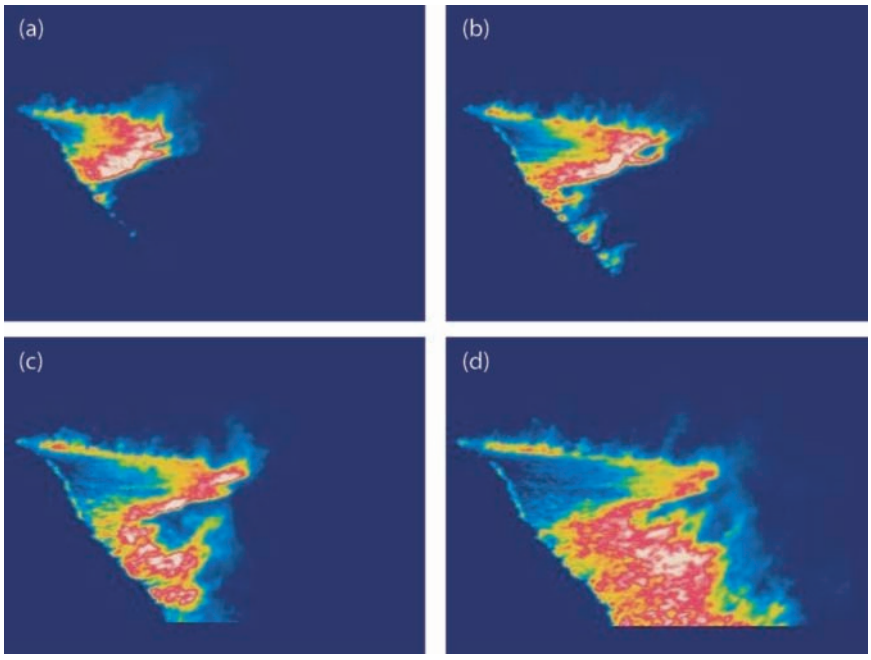

Fig. 4. Infrared image sequence covering the ignition of the experimental burn. Peak temperatures measured were (a) 796°, (b) 774°, (c) 760°, and (d) 834°C.

from outside of the plume. The temperature increase of the upper plume occurred much sooner than at the mid- (Fig. 6b) and lower (Fig. 6c) levels. As the lower plume and head fire approach the tower base, stronger (Fig. 5; 1246:32 and 1247:02 CST) increases in temperature occurred, as indicated in Fig. 6 in all panels. The maximum temperature measured within the plume was 295°C and occurred at a height of 4.5 m at 1246:45 CST (Fig. 6b) and corresponds to a time in the photos when the head fire is just passing the tower. This maximum represents plume temperature and not the in-fuel gas temperature associated with the actual fire. The maximum recorded temperature in the fuel was 751.5°C. This temperature was the temperature recorded at a height of 0.2 m near the base of the fuel bed. Radiation effects on the actual temperature are somewhat limited because of the relatively small diameter of the thermocouple and its placement within the dense grass fuel at the surface.

The tilted structure of the fire plume indicates an environment that is associated with wind shear. In addition, regions within the plume are much cooler and are associated with the entrainment of environmental air. These regions are indicated in Fig. 6 as sharp decreases in plume temperature as the plume passed the tower and indicate strong mixing within the entire depth of the plume. The tilted-plume structure during FireFlux is similar to that found during the pilot study (Clements et al. 2006).

Fig. 5. Photo time series of fire spread, fire behavior, and fire line propagation. Listed times are corrected to the data logger clock. Main tower is shown and is used as a reference point.

Observed flow and turbulence structure. Fire–atmosphere interactions create very complex flow structures near the earth's surface. The influence of the fire front on the surface layer during FireFlux is shown in Fig. 7 using a time series of 1-s-averaged 2-m wind and temperature obtained from the sonic anemometer and fine-wire thermocouple located on the main tower. There are a number of interesting features that warrant discussion. First, as the fire front approaches, the wind speed and direction change from ambient conditions such that the flow reverses and becomes calm, indicating the formation of a convergence zone ahead of the fire front. Surprisingly, the convergence zone forms for only a brief period (Fig. 7a; red arrow). Wind direction shifted from northeasterly to southerly at 1245:50 CST, approximately 50 s before the head fire reached the tower. As the fire front passed the tower (1246:40 CST; Fig. 5) wind direction then switched back to the ambient northerly flow and the wind speed nearly tripled in magnitude from approximately 3 to over 10 m s^{-1}. Coinciding with this increase in horizontal wind speed is a period of strong updrafts and

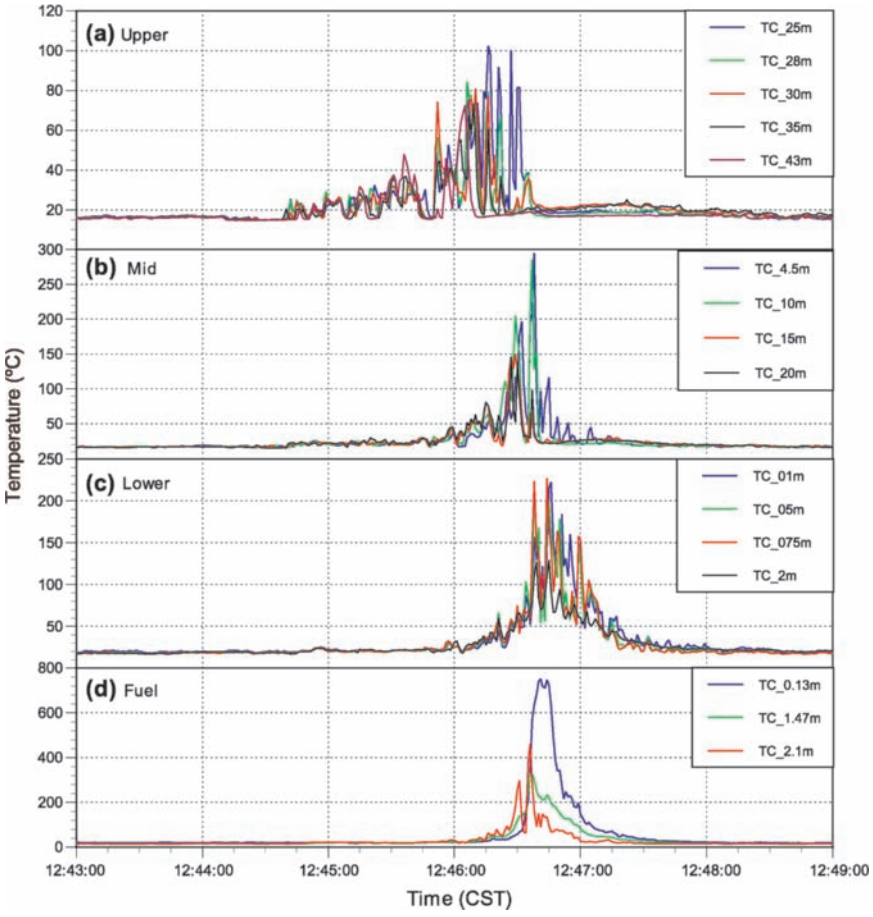

Fig. 6. Thermocouple measurements of temperature at different levels on the main tower, (a) the upper levels, (b) the midlevels, (c) the low levels, and (d) the fuel temperatures measured away from the tower.

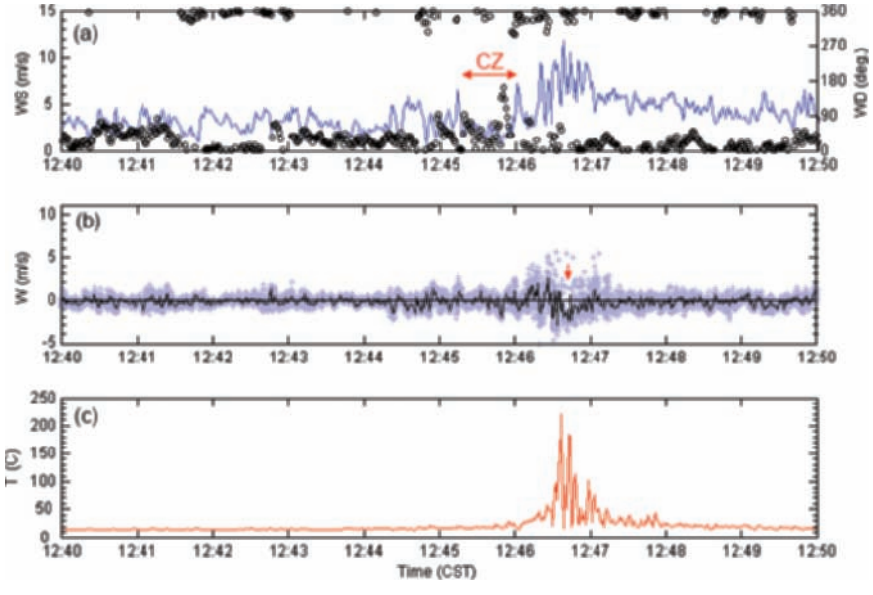

Fig. 7. Time series of 1-s average data from the 2-m sonic anemometer on the main tower. (a) Wind speed is indicated by the blue line and wind direction by black circles. (b) The vertical velocity, *w*, where blue crosses are the instantaneous 20-Hz tilt-corrected values and the solid black line is 1-s data. (c) Fine-wire thermocouple temperature (*T*). (a) The convergence zone is indicated by CZ. (b) The region of downdrafts is indicated with a small red arrow.

downdrafts reaching speeds of nearly 5 m s^{-1} (Fig. 7b). Just as the fire front passed the tower, a period of downward motion occurred, as indicated in Fig. 7b with the small red arrow. This period was compared to the video and time-lapse photography and is actually associated with the formation of a horizontal vortex immediately ahead of the fire front. This was visually indicated by soot particles dropping out in front of the head fire. Maximum 1-s-averaged temperatures at 2 m at the time of the fire front passage were on the order of 200°C, as measured by the fine-wire thermocouple, while the maximum sonic temperature was limited to the instrument limit of 50°C. Upper levels of the plume were associated with the strongest vertical velocities of ~10 m s^{-1} (not shown), when compared to surface values. The largest downward motion also occurred in the upper plume after the fire front passed. This consistent downward motion has also been shown in model simulations to occur behind the fire front (Sun et al. 2006).

Plume moisture concentrations can increase dramatically due to the combustion of the fuels from the fire (Potter 2005). Water-vapor mixing ratios obtained from the tethersonde system located immediately downwind of the burn area within the tolerable range of the tethersonde system, strong downdrafts pushed the balloon down and as it regained upward buoyancy, the force was strong enough to break the carabiner that connected the tetherline to the balloon. At this point all five tethersondes fell to the ground. Despite this loss, data up to that point show interesting plume features that warrant mention here. Water vapor mixing ratios were initially at 8 g kg^{-1} at 1030 CST, and began to decrease slightly to 7.5 g kg^{-1}. At approximately 1210 CST, the back burn along the southern edge of the prairie was initiated and the moderate plume associated with this had instantaneous mixing ratios at the 3-m level of up to 10.5–11.8 g kg^{-1} while 1-min-averaged values were on the order of only 8.5–9.0 g kg^{-1}. Mixing ratios obtained from the humidity probes on the main tower (not shown) indicated greater increases of up to ~2.5 g kg^{-1}, but for the main plume, which was much more intense than that produced by the back burn. These increases are important because they show the amount of moisture released due to the fire's consumption of native coastal grasses. Clements et al. (2006) showed similar increases from this prairie during the pilot study with much wetter surface conditions and less fire intensity.

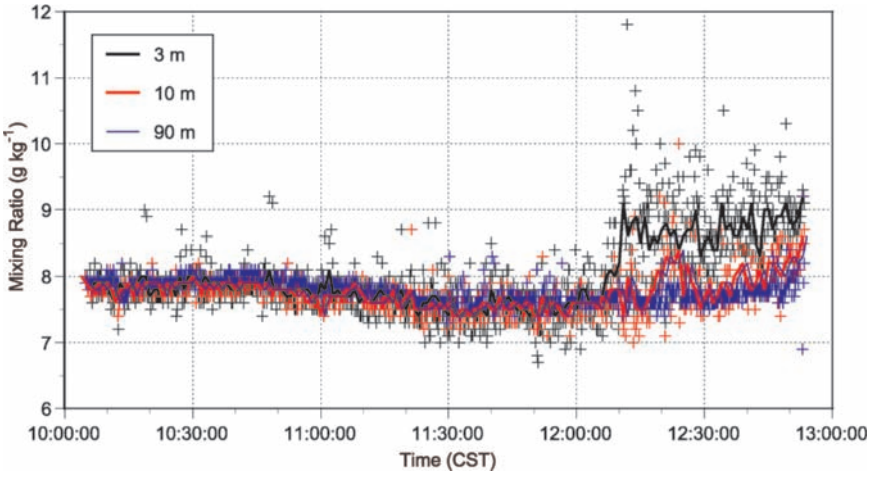

Fig. 8. Water vapor mixing ratio obtained from tethersonde system downwind of the burn unit during black lining operations. Solid lines are 1-min-averaged values and crosses are 10-s instantaneous values.

Figure 9 shows the time series of 1-min-averaged-sensible heat fluxes for each of the four levels on the main tower. The heat flux magnitude increases with height even though the lowest level closest to the fire front had the highest measured temperatures (Fig. 6). The magnitude of heat flux is greatest at 43 m, and there is a delay in the increases of heat flux on the lower levels. This delay is consistent with the observed temperatures measured by the thermocouples (Fig. 6). The maximum kinematic heat flux was ~25.8 K m s^{-1}, which is approximately 28.5 kW m^{-2}. While these large values seem high given the circumstance of the measurements, the in situ–measured fluxes are actually less than expected due to the maximum temperature limits of the sonic anemometry. We can estimate however, the heat flux using the observed values at 2 m of w ~5 m s^{-1} and the instantaneous values of the

are shown in Fig. 8. One-minute-averaged and 10-s instantaneous mixing ratio values are plotted from 1005 to 1255 CST. Data after this point are missing due to the loss of the tethered balloon as a result of strong vertical downdrafts during the initial plume impingement on the balloon. While maximum horizontal winds were similar to those observed at the main tower during fire passage (~10 m s^{-1}) and,

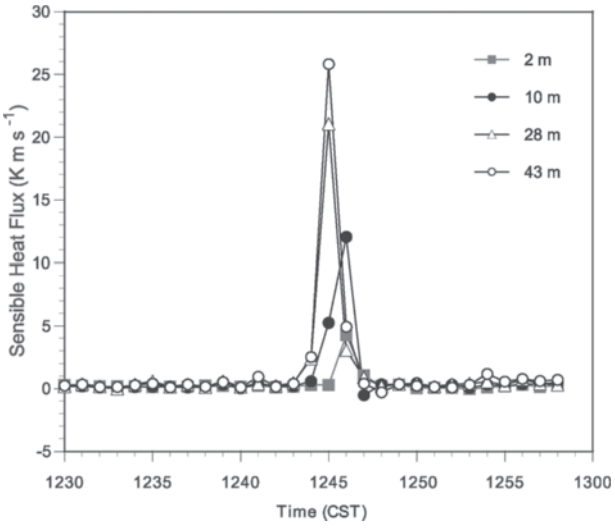

Fig. 9. Sensible heat fluxes calculated for each level of the main tower.

2-m fine-wire thermocouple, T_c, of ~200°C, to arrive at values of wT_c of about 1 MW m^{-2}. This magnitude is more reasonable for heat flux associated with moderate wildland fires and similar to that estimated by Clark et al. (1999).

Fire-induced flow. Observations of wind and temperature structure taken from all levels on the main tower provide a unique opportunity to develop a conceptual model of combustion-zone winds associated with a fast-moving head fire in tall grass fuel. First, the surface winds do not change in direction for more than a few seconds. For example, the winds shifted from north-northeast to southeasterly for only a few seconds, and then shifted to northwesterly before shifting back to the ambient flow direction of northeasterly. This may be due to the location of the apex of the head fire being very close and just to the west of the tower. Observers on the west flank of the fire noted very strong west-northwest winds as the head fire approached. Thus, an array of towers aligned east–west would have provided a better description of the surface flows and verification by direct observation of the convergence zone that should be present in the region just ahead or downwind of the fire front. While the wind direction did not change dramatically, the wind speed did. As the fire front approached, surface wind speed more than tripled. At the upper levels of the plume, there were large increases in wind speed, but not as long in duration as observed at the surface. Before the increase in wind speed occurred, there was a brief calm period that coincided with the initial increased updrafts. This calm period is associated with low-level convergence ahead of the fire line; however, this convergence zone was farther ahead of the fire than previously thought. At the time of fire front passage, horizontal wind speeds increased due to fire-induced circulations; background winds observed outside the burn perimeter (not shown) remained constant at this time.

Measurements from the south tower also indicate interesting fire-induced circulations ahead of the fire front. Figure 10 shows a similar time series to that shown in Fig. 7. At 1246:00 CST, 2-m-level winds shifted from northeasterly to easterly and then at ~1247:15 CST, the winds became calm and shifted to southerly, indicating inflow into the approaching fire front. This feature is very similar to that shown in Fig. 7 for the fire-induced winds. Soon after (~1248:15 CST), the winds became easterly

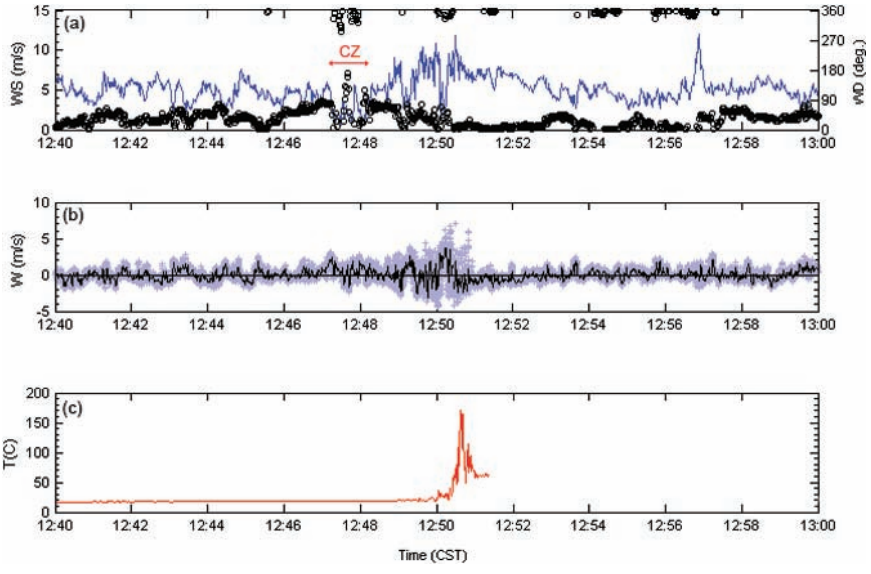

Fig. 10. Time series of 1-s average data from the 2-m sonic anemometer on the south tower. (a) Wind speed is indicated by the blue line and wind direction by black circles. (b) The vertical velocity, *w*, where blue crosses are the instantaneous 20-Hz tilt-corrected values and the solid black line is 1-s data. (c) Fine-wire thermocouple temperature (*T*). (a) The convergence zone is indicated by CZ.

and increased in magnitude to over 10 m s^{-1}. At 1250:10 CST the winds became calm again as vertical motion was very strong. Instantaneous upward vertical velocities were ~7 m s^{-1} and downward velocities were over 4 m s^{-1}. This motion is associated with the horizontal vortex that occurred immediately in front of the fire front as observed at the main tower. Just after the vortex passed the tower, the fire front passed as indicated by the dramatic increase in temperature (up to ~180°C). At ~1250:30 CST, winds immediately switched to a steady northerly flow while downward motion occurred for the next 1.5 minutes. This period is associated with the downdrafts that occur behind the fire front and horizontal winds that cross the fire line.

Mechanisms that are responsible for the formation of fire-induced winds have been discussed extensively in the literature (e.g., Church et al. 1980; Haines 1982; Heilman and Fast 1992; Heilman 1994; Clark et al. 1996; Sun et al. 2006). The modeling studies of Heilman and Fast (1992) and Clark et al. (1996) suggest that the convection column is linked to the fire at the surface and tilts in the downstream direction with height when ambient winds are present. This is observed in the tower thermocouple data (Fig. 6) as the plume impinges on the upper levels of the tower first. These modeling studies also suggest that the effect of the downstream tilting shifts the center of low-level convergence ahead of the fire front. If the convergence zone remains in front, but adjacent to the fire line, then the flow will be continuously induced across the fire line. More recently, Sun et al. (2006) suggested another mechanism for fire-induced winds. They show that fire-induced flow across the fire line is caused by downdrafts that are formed from the interaction between the fire plume and large eddies in the convective boundary layer. Their simulations show regions of convergence ahead of the fire line and areas of strong downdrafts directly behind the fire line that contribute to cross-fire line flow. They suggest that the role of the downdrafts is to bring higher momentum aloft to the surface, increasing the rate of fire spread.

Observations from FireFlux also indicate the presence of downdrafts just behind the fire front (Fig. 7). While Sun et al. (2006) present vertical velocities at 147 m AGL, our measurements are at 2, 10, 28.5, and 43 m AGL and indicate similar magnitudes. Their simulated plots are 3 times larger in length than the prairie burned during FireFlux and so a direct comparison may not be valid. The time series photos in Fig. 5 also show that at the time of the fire front passage, the upper levels of the tower were in clear air and indicate entrainment of air from aloft by downdrafts. Downward motion did, however, continue to occur sometime after the fire front had passed.

SUMMARY AND CONCLUSIONS. This paper presents an overview of a field experiment aimed at better understanding the atmospheric dynamics of wildland grass fires and providing a dataset for fire–atmosphere model development and validation. The FireFlux experiment represents the most intensively studied fire–atmosphere interactions associated with a grass fire to date. Preliminary results indicate that fire-induced flows are very complex and that large upward vertical motion on the order of 10 m s^{-1} can be associated with small grass fires while downward vertical motion occurs behind the fire line, confirming the simulations performed by Sun et al. (2006).

Key preliminary findings from this study include the following:

- Maximum measured sensible heat fluxes were ~28.5 kW m^{-2} and occurred in the upper plume rather than near the surface. However, estimated instantaneous near-surface heat fluxes were on the order of 1 MW m^{-2}.
- Observed fire-induced surface winds were 2–3 times the background ambient winds. A similar doubling in wind speed for fire-induced winds was observed through IR image analysis for intense crown fires (Coen et al. 2004).
- A convergence zone formed ahead of the fire line and was indicated by a surprisingly short period of very weak inflow at the surface.
- Observed instantaneous upward vertical velocities were on the order of 10 m s^{-1} and downward vertical velocities were ~5 m s^{-1}. Updraft velocities were similar in magnitude to those observed by Banta et al. (1992) for wildfires. While the updraft velocities of Coen et al. (2004) were stronger by a factor of around 2.5, the sensible heat flux from the crown fire was an order of magnitude greater.
- Fifty meters downwind of the burn perimeter, turbulent downdrafts at 130 m AGL were strong enough to push the tethered balloon downward to the point where the upward return motion broke the carabiner that attached the balloon to the tetherline.
- Vertical temperature structure showed that stronger temperature increases occurred at higher elevations much earlier than near the surface due to the forward tilting of the plume.

- Observations of soot falling just ahead of the fire front indicate strong downward motion near the surface that can be attributed to a horizontal roll vortex just in front of the head fire.
- Water-vapor mixing ratios increased ~1–2.5 g kg^{-1} within the plume as measured downwind of the burn unit, confirming similar results from Clements et al. (2006).

FireFlux produced a wealth of data, of which only a small fraction has been presented in this paper. More detailed analyses of the momentum, moisture, heat, and turbulent kinetic energy budgets associated with the head fire are planned in addition to a full analysis of the CO_2 measurements. A goal of FireFlux was to provide as comprehensive a dataset as possible on fire–atmosphere interactions that can be used for developing and validating the next generation of fire behavior tools. Modeling studies of the FireFlux burn are currently underway that hope to use FireFlux measurements to improve/validate model parameterizations. While the previous generation of fire behavior models was content at being able to describe the evolution of the fire front, the focus of the next generation of physics-based fire models is to get the evolution of the fire perimeter right for the correct reasons. Advancing the state of the science, which serves as the foundation upon which the next-generation fire models will be based, will allow fire managers to make more informed, scientifically sound decisions, and develop more effective fire management strategies that help protect property and save lives.

ACKNOWLEDGMENTS. The authors would like to thank burn bosses, Mark Kramer and George Regmond, and the trained volunteers from the Armand Bayou Nature Center for their hard work in managing and conducting the experimental burn. We thank Tim Becker from the Houston Coastal Center for helping with the experimental setup, fuel reduction treatments, and photography. We also thank Laura Hightower and Neil Jody for helping with the photography efforts. We would like to acknowledge Daewon Byun for his support of the research activities conducted at the Houston Coastal Center. This work is partially supported by a research grant from the Houston Coastal Center, EPA Grant (R-82906801) and the National Research Initiative Air Quality Program of the Cooperative State Research, Education, and Extension Service, U.S. Department of Agriculture, under Agreement 2004-05240. Use of trade names does not imply endorsement by the USDA Forest Service.

REFERENCES

Alexander, M. E., B. J. Stocks, B. M. Wutton, M. D. Flannigan, J. B. Todd, B. W. Butler, and R. A. Lanoville, 1998: The International Crown Fire Modeling Experiment: An overview and progress report. Preprints, *Second Symp. on Fire and Forest Meteorology,* Phoenix, AZ, Amer. Meteor. Soc., 20–23.

Anderson, H. E., 1982: Aids to determining fuel models for estimating fire behavior. General Tech. Rep. INT-122. U.S. Department of Agriculture, Forest Service, Intermountain Forest and Range Experiment Station, Ogden, UT, 22 pp.

Andrews, P. L., C. D. Bevins, and R. C. Seli, 2005: BehavPlus fire modeling system, version 3.0: User's guide revised. General Tech. Rep. RMRS-GTR-106WWW Revised, U.S. Department of Agriculture, Forest Service, Rocky Mountain Research Station, Ogden, UT, 132 pp.

Banta, R. M., L. D. Olivier, E. T. Holloway, R. A. Kropfli, B. W. Bartram, R. E. Cupp, and M. J. Post, 1992: Smoke-column observations from two forest fires using Doppler lidar and Doppler radar. *J. Appl. Meteor.,* **31,** 1328–1349.

Cheney, N. P., and J. S. Gould, 1995: Fire growth in grassland fuels, *J. Wildland Fire,* **5,** 237–347.

——, ——, and W. R. Catchpole, 1993: The influence of fuel, weather and fire shape variables on fire-spread in grasslands, *Int. J. Wildland Fire,* **3** (1), 31–44.

Church, C. R., J. T. Snow, and J. Dessens, 1980: Intense atmospheric vortices associated with a 1000-MW fire. *Bull. Amer. Meteor. Soc.,* **61,** 682–694.

Clark, T. L., M. A. Jenkins, J. Coen, D. Packham, 1996: A coupled atmosphere-fire model: role of the convective froude number and dynamic fingering at the fireline. *Int. J. Wildland Fire,* **6,** 177–190.

——, L. Radke, J. Coen, and D. Middleton, 1999: Analysis of small-scale convective dynamics in a crown fire using infrared video camera imagery. *J. Appl. Meteor.,* **38,** 1401–1420.

——, J. Coen, and D. Latham, 2004: Description of a coupled atmosphere-fire model. *Int. J. Wildland Fire,* **15** (3), 299–306.

Clements, C. B., B. E. Potter, and S. Zhong, 2006: In-situ measurements of water vapor, heat, and CO_2 fluxes within a prescribed grass fire. *Int. J. Wildland Fire,* **15** (3), 299–306.

Coen, J., S. Mahalingam, and J. Daily, 2004: Infrared imagery of crown-fire dynamics during FROSTFIRE. *J. Appl. Meteor.,* **43,** 1241–1259.

Finney, M. A., 1998. FARSITE: Fire Area Simulator-Model Development and Evaluation. Research Paper

RMRS-RP-4, Department of Agriculture, Forest Service, Rocky Mountain Research Station, Ogden, UT, 47 pp.

Haines, D. A., 1982: Horizontal Roll Vortices and Crown Fires, *J. Appl. Meteor.,* **21,** 751–763.

Heilman, W. E., 1994: Simulations of buoyancy-generated horizontal roll vortices over multiple heating lines. *Forest Sci.,* **40,** 601–617.

——, and J. D. Fast, 1992: Simulations of horizontal roll vortex development above lines of extreme surface heating. *Int. J. Wildland Fire,* **2** (2), 55–68.

Linn, R. R., and P. Cunningham, 2005: Numerical simulations of grass fires using a coupled atmosphere-fire model: Basic fire behavior and dependence on wind speed. *J. Geophys. Res.,* **110,** D13107, doi:10.1029/2004JD005597.

Potter, B. E., 2005: The role of released moisture in the atmospheric dynamics associated with wildland fires. *Int. J. Wildland Fire,* **14** (2), 77–84.

Radke, L. R., T. L. Clark, J. L. Coen, C. Alther, R. N. Lockwood, P. J. Riggin, J. Brass, and R. , 2000: The Wildfire Experiment (WiFE): Observations with airborne remote sensors. *Can. J. Remote Sens.,* **26,** 406–417.

Schotanus, P., F. T. M. Nieuwstadt, and H. A. R. DeBruin, 1983: Temperature measurement with a sonic anemometer and its application to heat and moisture fluctuations. *Bound.-Layer Meteor.,* **26,** 81–93.

Sun, R., S. K. Krueger, M. A. Zulauf, M. A. Jenkins, and J. J. Charney, 2006: Wildfire evolution in the convective boundary layer. Preprints, *17th Symp. on Boundary Layers and Turbulence,* San Diego, CA, Amer. Meteor. Soc., CD-ROM, 1.8A.

Tymstra C., M. D. Flannigan, O.B. Armitage, and K. Logan, 2007: Impact of climate change on area burned in Alberta's boreal forest. *Int. J. Wildland Fire,* **16,** 153–160.

Weaver, T., 2006: *A word to the firewise. Wildland Firefigher,* **10** (7), 25–30.

Wilczak, J. M., S. P. Oncley, and S. A. Stage, 2001: Sonic anemometer tilt correction algorithms. *Bound.-Layer Meteor.,* **99,** 127–150.

Wilmore, R., K. Slaughter, M. Theisen, and J. Roessler, 1998: FROSTFIRE research prescribed burn plan. Tech. Rep. Bureau of Land Management Alaska Fire Service, 62 pp.